Copper-related information from the oxygen 1*s* resonant x-ray emission in low-dimensional cuprates

Kozo Okada*
Department of Physics, Faculty of Science, Okayama University, 3-1-1, Tsushima-naka, Okayama, 700-8530, Japan

Akio Kotani
The Institute for Solid State Physics, University of Tokyo, Kashiwanoha 5-1-5, Kashiwa, Chiba 277-8581, Japan
(Received 11 September 2001; published 5 April 2002)

Incident- and outgoing-photon polarization dependences of O 1*s* x-ray emission spectrum (XES) in low-dimensional cuprate systems are investigated through model calculations using finite-size cluster models which include several copper sites. It is shown that the O 1*s* resonant XES provides information on the Cu-related excitations such as the Cu *dd* excitations and the charge-transfer (CT) excitations, in addition to the oxygen proper excitations. In particular, the lowest-energy CT between the neighboring CuO_4 plaquettes accompanies Zhang-Rice singlet formation. Even the Cu 3*d* spin flip can be observed as an inelastic scattering peak. Thus the O 1*s* resonant XES can be a nice tool to investigate metal-ion-related excitations in oxides.

DOI: 10.1103/PhysRevB.65.144530 PACS number(s): 74.72.−h, 78.70.En

I. INTRODUCTION

Core-level resonant x-ray emission spectroscopy (RXES) is one of the most powerful tools to obtain site-, element-, and orbital-selective information on the electronic states of strongly correlated electron systems, such as 3*d*, 4*f*, and 5*f* electron systems.[1] Combined analyses of core-level RXES at the cation and anion sites provide full information on the electronic structure of compounds. However, so far the RXES at the anion site has not been investigated so much both experimentally and theoretically, compared with that at the cation site. In the present study, we discuss what can be obtained from the RXES at the oxygen site in layered cuprates.

The resonant O 1*s* XES process under consideration is schematically shown in Fig. 1. An electron absorbing an incoming x ray is first excited to the so-called upper Hubbard band (UHB) which is a hybridized state of the Cu 3*d* and O 2*p* states. In the subsequent x-ray emission process, one of the O 2*p* electrons falls into the O 1*s* core hole. Roughly speaking, the emission intensity is expected to be proportional to the number of O 2*p* electrons. Indeed, it was confirmed in the study of layered cuprates,[2–4] where the obtained spectra were compared with the partial density of states obtained by energy-band calculations. Note that the chemical shift of the O 1*s* levels was utilized to distinguish the contributions from nonequivalent oxygen sites in their studies.

In more detail, however, RXES does not coincide with the O 2*p* partial density of states owing to the selection rule for the RXES process, as shown later from a group-theoretical point of view. Moreover, we would like to stress that O 1*s* RXES will also provide information on Cu-related electronic states, since the O 2*p* and Cu 3*d* states are well hybridized owing to the strong *pd* hybridization. The first attempt to observe Cu-related excitations in $CuGeO_3$ by means of O 1*s* RXES has been done by Duda *et al.*[5] They have shown that O 1*s* RXES could provide information on the Cu 3*d* states, such as the *dd* excitations and Zhang-Rice singlet (ZRS) formation.[5,6] In other words, O 1*s* RXES can be a tool to investigate the many-body states in cuprate systems.

To the present authors' knowledge, on the other hand, there are only a few many-body theoretical studies of the O 1*s* RXES in cuprates, which were given by the present authors.[7,8] As for so-called edge-sharing-type structures, such as $CuGeO_3$ and Li_2CuO_2, we predicted a novel inter-CuO_4-plaquette charge-transfer (CT) mechanism via a core-hole state.[7] As for corner-sharing-type structures, such as La_2CuO_4 and $Sr_2CuO_2Cl_2$, we predicted, as a short report, a remarkable polarization dependence of O 1*s* RXES.[8] In the present study, we show, in more detail, how to understand the characteristic features in O 1*s* RXES, paying attention to undoped corner-sharing cuprates. This is a first step to understand the O 1*s* RXES in cuprates and is a basis to extend the analysis to doped cuprates and noncuprate systems. In particular, we concentrate on the cuprates with no apical oxygen, such as $Sr_2CuO_2Cl_2$, since all oxygen sites are equivalent. This can be helpful and important when we compare the theory and experiments in the future.

The rest of the present paper is organized as follows: In Sec. II, we describe our model Hamiltonian which is a multiband Hubbard model Hamiltonian combined with a core-

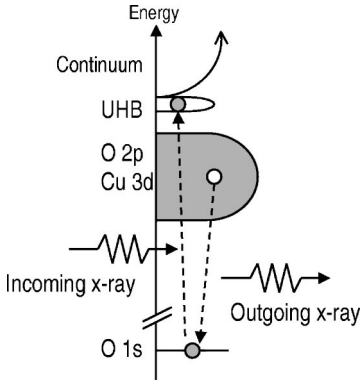

FIG. 1. Resonant x-ray emission at the O site in cuprates.

 ©2002 The American Physical Society

hole potential term. In Sec. III, we first show the analytic results for CuO_4 clusters, which give the fundamentals in understanding the O 1*s* RXES both for corner- and edge-sharing systems. For instance, it will be shown that the Cu *dd* excitations in O 1*s* RXES can be explained by means of CuO_4 clusters. In multi-Cu-site clusters, such as Cu_2O_7 and Cu_4O_{12}, on the other hand, it will be shown that a ZRS excitation can be formed in the RXES final state. In Cu_4O_{12}, an inelastic scattering peak due to the two-Cu-spin flip (or two-spin exchange) is also predicted. In Sec. IV, we discuss the points in comparing with the experiments and summarize our results.

II. MODEL

The Hamiltonian consists of a conventional *dp* Hamiltonian and a core-related one:

$$H = H_{pd} + H_{\rm core}. \tag{1}$$

The former is given in the hole picture by

$$\begin{aligned} H_{pd} = & \sum_{i,\gamma,\sigma} \varepsilon_{d,\gamma} n_{d,i\gamma\sigma} + \sum_{j,\alpha\sigma} \varepsilon_p n_{p,j\alpha\sigma} \\ & + \sum_{\langle i,j\rangle\gamma,\alpha,\sigma} V_{pd,ij} (d^\dagger_{i\gamma\sigma} p_{j\alpha\sigma} + p^\dagger_{j\alpha\sigma} d_{i\gamma\sigma}) \\ & + \sum_{\langle j,j'\rangle,\alpha,\alpha',\sigma} V_{pp,j\alpha j'\alpha'} (p^\dagger_{j\alpha\sigma} p_{j'\alpha'\sigma} + p^\dagger_{j'\alpha'\sigma} p_{j\alpha\sigma}) \\ & + \sum_{i,(\gamma\sigma>\gamma'\sigma')} U_{dd} n_{d,i\gamma\uparrow} n_{d,i\gamma'\downarrow}, \end{aligned} \tag{2}$$

where $d^\dagger_{i\gamma\sigma}$ ($p^\dagger_{j\alpha\sigma}$) creates a hole on the *i*th Cu site (the *j*th O site). Here γ and α are orbital indexes and σ specifies the spin state. The first and second terms on the right-hand side of Eq. (2) represent the one-body energies, where $n_{d,i\gamma\sigma}$ ($n_{p,j\gamma\sigma}$) is the number operator for the Cu 3*d* (O 2*p*) hole. In the present paper, we define the CT energy as $\Delta = \varepsilon_p - \varepsilon_{d,x^2-y^2}$. The third term represents the hybridization of the Cu 3*d* and O 2*p* orbits, where $\langle i,j\rangle$ denotes the summation over the nearest-neighbor pairs. The fourth term represents the hybridization of the neighboring O 2*p* orbits. The last term represents the Coulomb repulsion between Cu 3*d* holes.

The core-related Hamiltonian is given by

$$H_{\rm core} = \sum_{j,\sigma} \varepsilon_c n_{c,j\sigma} + \sum_{j,\alpha,\sigma,\sigma'} U_{pc} n_{p,j\alpha\sigma'} n_{c,j\sigma}, \tag{3}$$

where n_c is the number operator for the O 1*s* core hole. For simplicity the first term on the right-hand side of Eq. (3) is the one-body energy of the O 1*s* core state. The second term describes the Coulomb interaction between the O 1*s* and 2*p* holes.

The relevant part of the RXES spectral function is given by the following expression:[1]

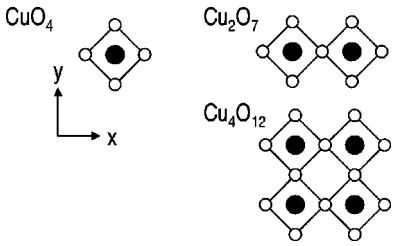

FIG. 2. Cluster models used in the present study are shown, where the open and solid circles represent O and Cu sites, respectively.

$$I_{\nu\mu}(\omega_{out},\omega_{in}) = \sum_f \left| \sum_{m,\sigma} \frac{\langle f|H_\nu|m\rangle\langle m|H_\mu|g\rangle}{E_g+\omega_{in}-E_m+i\Gamma_m} \right|^2 \times \delta(E_g+\omega_{in}-E_f-\omega_{out}), \tag{4}$$

where ω_{in} and ω_{out} are the incident and emitted photon energies and μ and ν are their polarization directions, respectively. $|g\rangle$, $|m\rangle$, and $|f\rangle$ represent the ground (initial), intermediate, and final states of the system, respectively, and the corresponding energies are E_g, E_m, and E_f. The core-hole lifetime broadening effect in the intermediate state is taken into account by a constant parameter Γ_m (=0.5 eV). The dipole transition is caused by

$$H_\mu = \sum_{j,\sigma} s^\dagger_{j\sigma} p_{j\mu\sigma} + p^\dagger_{j\mu\sigma} s_{j\sigma}. \tag{5}$$

In numerical calculations for $(Cu_2O_7)^{10-}$ and $(Cu_4O_{12})^{16-}$ clusters, we adopt the Lanczos method[10] to diagonalize *H* in order to treat the electron correlation as exactly as we can. The RXES spectrum is obtained by the numerical integration of the generating function.[11]

III. RESULTS OF NUMERICAL CALCULATIONS

A. CuO_4 cluster

Since a square-planar $(CuO_4)^{-6}$ cluster with D_{4h} point symmetry, which is shown in Fig. 2, has only a single valence hole in the ground state, we can obtain analytic results easily. On the basis of configuration-interaction (CI) picture,[9] the ground state is a linear combination of $d^9(x^2-y^2)$ and $d^{10}\underline{L}(x^2-y^2)$ electron configurations, where $\underline{L}(x^2-y^2)$ denotes a ligand hole (O 2*p* hole) with x^2-y^2 symmetry (B_{1g} irreducible representation in D_{4h} point symmetry).

X-ray absorption occurs in the present CuO_4 cluster, when the electric field vector of the x-ray is in the *xy* plane. Since $B_{1g}\times E_u = E_u$, the symmetry of the resultant O 1*s* core-hole state (molecular orbit state) is E_u.

In the subsequent x-ray emission process, one of the O $2p_{x,y,z}$ electrons falls into the core-hole state. In the case of the x-ray emission with *z* polarization, the symmetry of the resultant valence-hole states is E_g, since $E_u\times A_{1u} = E_g$. In the case of the *x* or *y* polarization, the symmetry of the resultant valence-hole states is given as follows: $E_u\times E_u = A_{1g}+A_{2g}+B_{1g}+B_{2g}$. The O 2*p* molecular-orbit state with A_{2g} symmetry does not mix with the Cu 3*d* states. For instance, the XES process which gives I_{xx} is shown in Fig. 3,

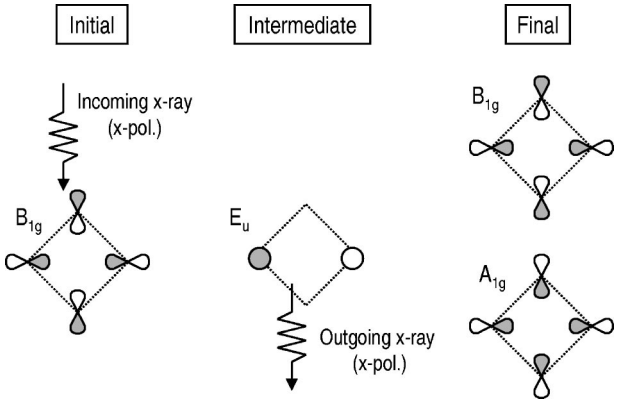

FIG. 3. O 1*s* resonant XES process which gives I_{xx} for CuO_4 is schematically shown.

where the symmetry of the hole state in the final states is A_{1g} or B_{1g}.

For $\Gamma = A_{1g}$, B_{1g}, B_{2g}, and E_g, the wave functions are described by linear combinations of $d^9(\Gamma)$ and $d^{10}\underline{L}(\Gamma)$ as

$$|f_\Gamma\rangle = \sin\theta_\Gamma |d^9(\Gamma)\rangle + \cos\theta_\Gamma |d^{10}\underline{L}(\Gamma)\rangle, \tag{6}$$

where θ_Γ is to be determined by diagonalizing the Hamiltonian

$$H_\Gamma = \varepsilon_{d,\Gamma}|d^9(\Gamma)\rangle\langle d^9(\Gamma)| + \varepsilon_{p,\Gamma}|d^{10}\underline{L}(\Gamma)\rangle\langle d^{10}\underline{L}(\Gamma)| + V_{pd,\Gamma}\{|d^9(\Gamma)\rangle\langle d^{10}\underline{L}(\Gamma)| + \text{H. c.}\}. \tag{7}$$

In Eq. (7), the origin of the energy levels is taken at the d^{10} state. The hybridization matix element $V_{pd,\Gamma}$ is given by $\sqrt{3}(pd\sigma)$, $-(pd\sigma)$, $2(pd\pi)$, and $\sqrt{2}(pd\pi)$ for $\Gamma = B_{1g}$, A_{1g}, B_{2g}, and E_g, respectively. This anisotropy in hybridization is the origin of the crystal field (CF) splitting of Cu 3*d* levels in the present calculation.

In the present case, since $\varepsilon_{d,\Gamma} < \varepsilon_{p,\Gamma}$, the lower-energy eigenstate is mainly $d^9(\Gamma)$. For $\Gamma = B_{1g}$, it is equivalent to the ground state and, accordingly, gives the elastic scattering peak. The other final states give inelastic scattering (IS) peaks. The XES intensity is proportional to the $d^{10}\underline{L}(\Gamma)$ weight in each final state, which is sensitive to Δ, $(p\bar{d}\sigma)$, and $(pd\pi)$. If one introduces the electrostatic crystal field splitting, such as $10Dq$, it also affects the XES intensity, as shown later. The O 1*s* RXES thus calculated are plotted as bars in Fig. 4. The abscissa is the x-ray energy shift $\Delta\omega$ $(\equiv \omega_{out} - \omega_{in})$. The parameter values used are as follows: $\Delta = 2$ eV, $(pd\sigma) = -1.5$ eV, $(pd\pi) = 0.7$ eV, $(pp\sigma) = 0.4$ eV, and $(pp\pi) = 0.12$ eV.

For instance, I_{xx} consists of the elastic peak and three IS peaks. The A_{1g} peak at -1.25 eV is mainly d^9. In other words, this A_{1g} peak corresponds to the *dd* excitation from x^2-y^2 to $3z^2-r^2$. The magnitude of the excitation energy is due to the anisotropic *pd* hybridization. On the other hand, two IS peaks located at around -5.5 eV correspond to the CT excitations. The CT excitation with B_{1g} symmetry is also observed in the Cu 1*s* RXES.

In the case of I_{yx}, there are three IS peaks. The B_{2g} peak at -1.33 eV is the *dd* excitation and that at -5.3 eV is due to CT. The energy difference between the A_{1g} and B_{2g} *dd* excitation peaks is also due to the anisotropic hybridization.

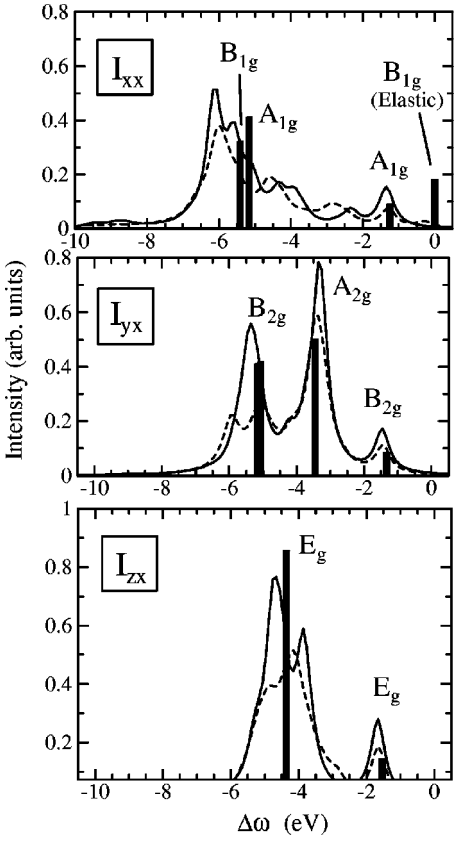

FIG. 4. O 1*s* resonant XES (I_{xx}, I_{yx}, and I_{zx}) in $(CuO_4)^{6-}$ (bars), $(Cu_2O_7)^{10-}$ (solid curves), and $(Cu_4O_{12})^{16-}$ (dashed curves). The abscissa is the x-ray energy shift $\Delta\omega$ $(\equiv \omega_{out} - \omega_{in})$. For the latter two cases, the spectrum is convoluted with a Lorentz function of width 0.5 eV, neglecting the elastic component.

For $\Gamma = A_{2g}$, the hybridization of the O 2*p* and Cu 3*d* wave functions does not occur. However, the position of this A_{2g} IS peak depends on the *pd* hybridization, since it is given by $E(A_{2g}) = \Delta - 2t_{pp} - E_g$, where E_g is the ground-state energy which is obtained by diagonalizing Eq. (7) for $\Gamma = B_{1g}$.

In Fig. 4, only five peaks located in between -5.5 eV and -3.5 eV contribute to the O 1*s* RXES. Note that their intensity distribution does not coincide with the O 2*p* partial density of states which is obtained by the energy-band calculations. This is because, as mentioned above, the O 2*p* molecular orbit (MO) states which can fall into the O 1*s* hole state are limited to those with A_{1g}, A_{2g}, B_{1g}, B_{2g}, or E_g symmetry. The O 2*p* MO states with A_{2u}, B_{2u}, or E_u do not contribute to the O 1*s* RXES. We also note that, in the case of the NXES where a photoexcited electron in the intermediate state enters a (non-UHB) continuum state and does not interact with the other electrons, all the O 2*p* electrons can fall into the core hole. Since the O 2*p* MO states with A_{2u}, B_{2u}, and E_u symmetry are of nonbonding-type, they contribute to the energy region close to A_{2g} and accordingly the intensity of the nonbonding O 2*p* band becomes large. The spectral features characteristic of RXES, such as the *dd* ex-

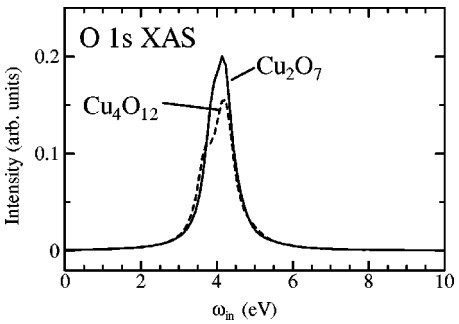

FIG. 5. O 1*s* XAS in $(Cu_2O_7)^{10-}$ (solid curve) and $(Cu_4O_{12})^{16-}$ (dashed curve). The origin of ω_{in} is taken at ε_c. The total intensity reflects the average O $2p$ hole number. Half the spectral width comes from the O 1*s* core-hole lifetime.

citation peaks and the B_{1g} CT peak, are likely to be hidden under the nonbonding O $2p$ band.

Hereafter the peaks ranging from -6 eV to -3 eV are called "O$2p$ main band," while those ranging from -3 eV to -1 eV "dd peaks."

B. Multisite clusters

In order to make our model more realistic, we must extend the cluster size. In this subsection, we show the calculated results for multi-Cu-site cluster models $(Cu_2O_7)^{10-}$ and $(Cu_4O_{12})^{16-}$.

There are two and four valence holes in $(Cu_2O_7)^{10-}$ and $(Cu_4O_{12})^{16-}$, respectively. The eigenstates for the present Hamiltonian are classified by the z component of the total spin S_z. In the present Hamiltonian, the ground state is given by the lowest-energy state in the $S_z=0$ subspace for both $(Cu_2O_7)^{10-}$ and $(Cu_4O_{12})^{16-}$. This is often explained by the superexchange coupling mechanism between the localized Cu $3d$ spins.

The O 1*s* XAS (x polarization) calculated for $(Cu_2O_7)^{10-}$ and $(Cu_4O_{12})^{16-}$ are plotted in Fig. 5. In addition to the parameter values used for CuO_4, $U_{dd}=8$ eV, $U_{pp}=4$ eV, and $U_{pc}=5$ eV are also used. The O 1*s* core-hole lifetime is assumed to be 0.5 eV. Since the calculated spectral width is about 1 eV, half the width is caused by the upper Hubbard bandwidth. Although a fairly large O 1*s* core potential (U_{pc}) is used, its effect on the XAS is quite small. This is because the average O $2p$ hole number is too small. It is less than 0.1 per O site and per spin. We note that the difference in the integrated intensity of XAS for $(Cu_2O_7)^{10-}$ and $(Cu_4O_{12})^{16-}$ is due to the fact that the x and y directions are equivalent on the latter cluster, while not on the former. This difference is also reflected in the integrated intensity of I_{xx}, I_{yx}, or I_{zx} shown in Fig. 4.

In Fig. 4, we show I_{xx}, I_{yx}, and I_{zx} in $(Cu_2O_7)^{10-}$ and $(Cu_4O_{12})^{16-}$ at $\omega_{in}=4.2$ eV (on resonance), where the spectra are convoluted with a Lorentz function of width 0.5 eV, neglecting the elastic component. As for the spectral distribution, we can see a rough correspondence between CuO_4 and the other two at a glance. With increasing the cluster size, the peaks which form the O$2p$ main band are split. In particular on going from CuO_4 to Cu_2O_7, the effect on I_{xx}

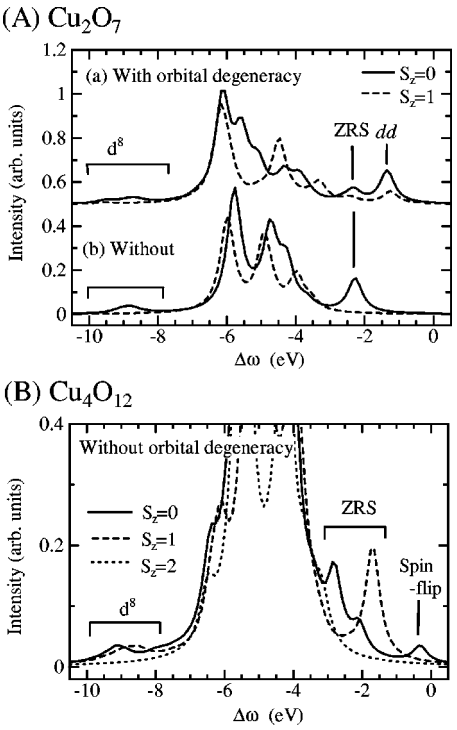

FIG. 6. (A) I_{xx} is calculated for $(Cu_2O_7)^{10-}$ with and without orbital degeneracy. In each case, the solid and dashed curves are obtained by using the $S_z=0$ and $S_z=1$ initial states, respectively. The former is the same as that shown in Fig. 4. (B) I_{xx} in $(Cu_4O_{12})^{16-}$ without orbital degeneracy is calculated for various S_z values.

appears to be very large. Therefore the CuO_4 single-site cluster model analysis cannot be used for discussing the line shape quantitatively. We note, on the other hand, that the dd peaks in I_{yx} and I_{zx} do not split. This is quite reasonable since the dd excitation occurs within a single CuO_4 plaquette.

As a result of extending the cluster size, there appears a new structure at around -9 eV in I_{xx}. From its U_{dd} dependence, we can easily see that it is caused by the d^8 final state.

As for I_{xx}, a peak close to the A_{1g} dd peak at around -2.5 eV is to be noted as a new one, though the position differs slightly for Cu_2O_7 and Cu_4O_{12}. In order to clarify its origin, the effects of the Cu $3d$ orbital degeneracy and the spin symmetry of the initial state are examined in Fig. 6. The solid curve in Fig. 6(A-a) is the same as that in Fig. 4. If we disregard the Cu $3d$ orbital degeneracy, only the peak denoted as "dd" disappears, as seen in Fig. 6(A-b). It is evident that the peak at -2.3 eV, which is denoted as "ZRS" (Zhang-Rice singlet) is not due to the A_{1g} dd excitation. We note here that the ZRS and dd excitations are coupled with each other to some extent owing to the symmetry of the Cu_2O_7 cluster. This is the reason for the weak ZRS peak in Fig. 6(A-a), compared with that in Fig. 6(A-b).

If we use the lowest energy state in the $S_z=1$ subspace as the initial state of the XES process, the ZRS peak also disappears, as shown in Fig. 6(A-b). It means that the $S_z=0$ spin configuration in the initial state is essential in giving the ZRS peak. The XES process which gives the ZRS peak is

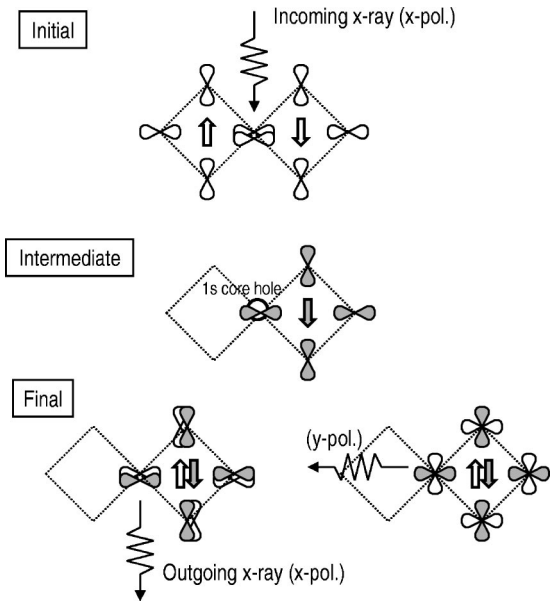

FIG. 7. XES process which causes interplaquette CT is illustrated. In the x-ray emission with *x* polarization, the ZRS is created in the right-hand-side CuO_4 plaquette.

illustrated in Fig. 7, where the up- and down-spin holes are localized on the left- and right-hand-side (RHS) plaquette, respectively, and the XES process is assumed to occur only at the O site which connects two Cu sites for simplicity. If the up-spin valence hole is annihilated in the x-ray absorption, the ZRS can be formed in the RHS plaquette for the x-ray emission with *x* polarization. In the case of the x-ray emission with *y* polarization, the energy of the resultant final state is higher than the ZRS. From this figure, it is obvious that the ZRS can be observed in I_{xx}.

We note that the ''ZRS'' state in the present case does not mean the one introduced by hole doping, since the total hole number is conserved through the XES process. The ''ZRS'' excitation in the present case is the interplaquette CT excitation from $|d^9;d^9\rangle$ to $|d^9\underline{L}(\mathrm{ZRS});d^{10}\rangle$.

In Fig. 6(B), I_{xx} in $(Cu_4O_{12})^{16-}$ without orbital degeneracy is calculated for various S_z values. In the case with $S_z=2$, which means that all valence holes take the same spin direction, there is no peak in the dd peak region. On the other hand, in the cases with $S_z=0$ and 1, the ZRS peak appears, though the energy position differs slightly for $S_z=0$ and 1. One reason for the difference may be a ''finite-cluster-size'' effect, and the other may be the intrinsic ZRS bandwidth effect.

In Fig. 6(B) (as well as in Fig. 4), we note that there is a new peak at around -0.3 eV in the $S_z=0$ case. The magnitude of the excitation energy suggests that the excitation is caused by the superexchange interaction between neighboring Cu $3d$ spins. The result that it is seen in $(Cu_4O_{12})^{16-}$ and not in $(Cu_2O_7)^{10-}$ indicates that it can be understood as the transition in the Cu spin configuration from $\uparrow\downarrow\uparrow\downarrow$ to $\uparrow\uparrow\downarrow\downarrow$ for instance.

C. Polarized and depolarized configurations

In actual experiments, outgoing x rays are usually detected in the direction perpendicular to the wave vector of incident x rays. The experimental configuration is called ''polarized'' when the electric field vector of incoming x rays is normal to the scattering plane, while it is called ''depolarized'' when the electric field vector is in the scattering plane. The XES at the polarized and depolarized configuration for *x*-polarized incident x rays can be obtained by taking linear combinations of I_{xx}, I_{yx}, and I_{zx}. In the normal incidence, which means that incident x rays come along the *z* axis in the present case, the XES at the polarized configuration (hereafter called the ''polarized spectrum'') is given by $I_{xx}+I_{zx}$ and that at the depolarized configuration (hereafter called the ''depolarized spectrum'') is given by $I_{yx}+I_{zx}$. In grazing incidence, which means that incident x rays come along the xy plane in the present case, the polarized spectrum is given by $I_{xx}+I_{yx}$ and the depolarized one is the same as that in the normal incidence $(=I_{yx}+I_{zx})$.

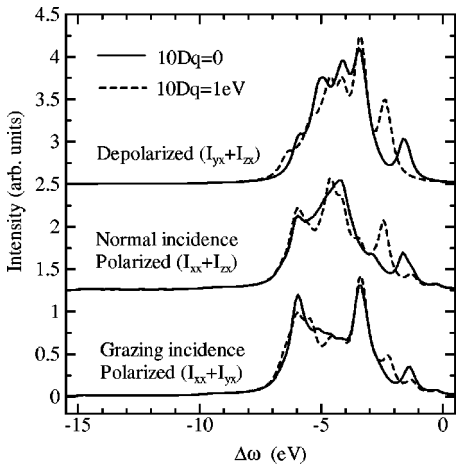

FIG. 8. O 1*s* RXES for polarized and depolarized configurations in $(Cu_4O_{12})^{16-}$. The depolarized spectrum is the same for the normal and grazing incidence. The solid curves are obtained from I_{xx}, I_{yx}, and I_{zx} shown in Fig. 4. The dashed curves are obtained for $10Dq=1$ eV.

The polarized and depolarized spectra for $(Cu_4O_{12})^{16-}$ shown in Fig. 8 are obtained from I_{xx}, I_{yx}, and I_{zx} shown in Fig. 4. The characteristic features can be interpreted by means of I_{xx}, I_{yx}, and I_{zx}. We note that both in the normal and grazing incidences the structure at around 6 eV is always conspicuous in the polarized spectrum, which is caused by the B_{1g} and A_{1g} CT peaks in I_{xx}.

Since the ZRS peak is seen only in I_{xx}, it can be observed only in the polarized configuration for both the normal and grazing incidences. In the former, for instance (solid curve in Fig. 8), a weak peak at -2.8 eV is due to the ZRS. On the other hand, a structure centered at -1.5 eV consists of the A_{1g} and E_g dd excitations. In the latter, the ZRS peak is hidden under the tail of the A_{2g} peak centered at -3.5 eV.

In Fig. 8, the spectra calculated with an additional electrostatic CF $(10Dq)$ are also shown for comparison. In the present calculation, $10Dq$ is introduced as an additional one-body energy for Cu $3d(E_g)$ and $3d(B_{2g})$ orbits, which means that the CT energy for E_g (and B_{2g}) is decreased by $10Dq$. Accordingly, in the polarized spectrum for the normal incidence, $10Dq$ does not affect the position of the A_{1g} dd

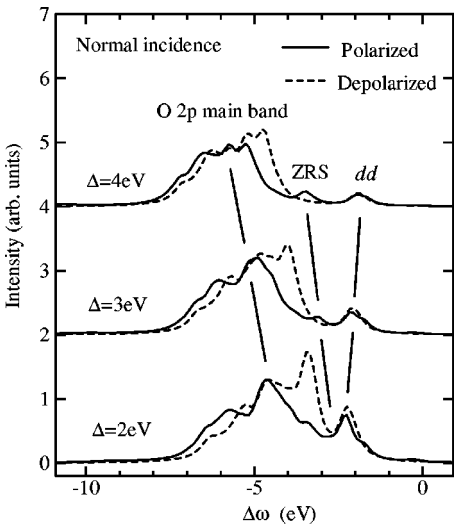

FIG. 9. Δ dependence of the O 1*s* RXES in $(Cu_4O_{12})^{16-}$ for normal incidence. In these calculations, the electrostatic CF of 0.8 eV is applied to the 3*d* states with A_{1g}, B_{2g}, or E_g symmetry.

peak and only the E_g *dd* peak moves to the lower-energy side with increasing the intensity. Thus the intensity distribution in the *dd* peak region is sensitive to $10Dq$ for instance. This point can be important in discussing the details of the experiment in future.

IV. DISCUSSION AND SUMMARY

In the present paper, we have clarified the origin of the characteristic features in O 1*s* RXES. As mentioned above, the details of the line shape depend on various parameters.

As mentioned above, the position of the O 2*p* main band as a whole is determined by Δ and *pd* hybridization. Moreover, the position of B_{1g} CT peak is also sensitive to these parameters. For instance, we show the Δ dependence of the O 1*s* RXES in Fig. 9, where an additional electrostatic CF of D_{4h} type is introduced. The O 2*p* main band shifts monotonically with Δ, while the CF splittings decrease slightly owing to the decreased hybridization effect. It is to be noted that the intensity of *dd* peaks decreases with Δ. This is because the $d^{10}\underline{L}$ weight in the final-state wave function for each *dd* peak decreases with Δ. Thus O 1*s* RXES provides direct information on Δ.

We have shown that O 1*s* RXES is a nice tool to investigate Cu-related electronic excitations, such as ZRS, *dd*, and two-spin-flip excitations. We emphasize the importance of the polarization-dependent experiments. The polarization dependence of the ZRS and *dd* peaks is summarized in Table I. A detailed experiment in future will enable us to discriminate these excitations. The B_{1g} CT excitation, which can be observed in the polarized configuration, also provides important information in determining the relevant physical parameters.

TABLE I. Polarization dependence of ZRS and *dd* excitations.

Incidence	Geometry	Detectable excitations
Normal	Polarized	ZRS, A_{1g}, E_g
	Depolarized	E_g, B_{2g}
Grazing	Polarized	ZRS, A_{1g}, B_{2g}
	Depolaized	E_g, B_{2g}

In principle, these excitations can also be detected in the RXES at a Cu site. For instance, ZRS and CT excitations can be observed in Cu 1*s* (3*s*) RXES (Refs. 12 and 13) and *dd* excitations can be observed in Cu 2*p* (3*p*) RXES.[14,15] Therefore O 1*s* RXES can be used to check the RXES at a Cu site. It is also to be noted that O 1*s* RXES is almost free from the core-hole effects which include multiplet and spin-orbit coupling effects, which are often important in the core-level spectra at a Cu site and which often make the spectral analysis difficult and complicated. It may be also important that the excitation energy of the O 1*s* level is much smaller than the Cu 1*s* and 2*p* levels, since it affects the experimental resolution. Furthermore, the intensity of the elastic peak of the O 1*s* RXES is much weaker than that of Cu 1*s*, 2*p*, and 3*p* RXES, so that O 1*s* RXES is more appropriate to observe inelastic excitations with small energy. For these reasons, O 1*s* RXES should be utilized more and more in the study of correlated electron systems.

ACKNOWLEDGMENTS

The present authors thank Professor S. Shin and Dr. Y. Harada for useful discussions and for providing their experimental data before publication. The paper was completed during one of the authors' (A.K.) visits to National Synchrotron Light Source in Brookhaven National Laboratory, and he thanks Dr. C. C. Kao for the invitation and discussion. This work was carried out by joint research at the Institute for Solid State Physics, the University of Tokyo.

*Electronic address: okada@science.okayama-u.ac.jp

[1] See, for instance, A. Kotani and S. Shin, Rev. Mod. Phys. **73**, 203 (2001).
[2] J.-H. Guo, S.M. Butori, N. Wassdahl, P. Skytt, E.J. Nordgren, and Y. Ma, Phys. Rev. B **49**, 1376 (1994).
[3] S.M. Butorin, J.-H. Guo, N. Wassdahl, P. Skytt, E.J. Nordgren, Y. Ma, C. Ström, L.-G. Johansson, and M. Qvarford, Phys. Rev. B **51**, 11 915 (1995).
[4] S.M. Butorin, J. Guo, N. Wassdahl, and E.J. Nordgren, J. Electron Spectrosc. Relat. Phenom. **110-111**, 235 (2000).
[5] L.-C. Duda, J. Downes, C. McGuinness, T. Schmitt, A. Augustsson, K.E. Smith, G. Dhalenne, and A. Revcolevschi, Phys. Rev. B **61**, 4186 (2000).
[6] F.C. Zhang and T.M. Rice, Phys. Rev. B **37**, 3759 (1988).
[7] K. Okada and A. Kotani, Phys. Rev. B **63**, 045103 (2001).
[8] K. Okada and A. Kotani, J. Synchrotron Radiat. **8**, 243 (2001).
[9] G. van der Laan, C. Westra, C. Haas, and G.A. Sawatzky, Phys. Rev. B **23**, 4369 (1981).
[10] See, for examle, V. Heine, in *Solid State Physics*, edited by H.

Ehrenreich, F. Seitz, and D. Turnbull (Academic Press, New York, 1980), Vol. 35, p. 87.

[11] S. Tanaka and Y. Kayanuma, Solid State Commun. **100**, 77 (1996).

[12] J.P. Hill, C.-C. Kao, W.A.L. Caliebe, M. Matsubara, A. Kotani, J.L. Peng, and R.L. Greene, Phys. Rev. Lett. **80**, 4967 (1998).

[13] P. Abbamonte, C.A. Burns, E.D. Isaacs, P.M. Platzman, L.L. Miller, S.W. Cheong, and M.V. Klein, Phys. Rev. Lett. **83**, 860 (1999).

[14] P. Kuiper, J.-H. Guo, C. Sathe, L.-C. Duda, and J. Nordgren, Phys. Rev. B **80**, 5204 (1998).

[15] L.-C. Duda, J. Nordgren, G. Dräger, S. Bocharov, and Th. Kirchner, J. Electron Spectrosc. Relat. Phenom. **110-111**, 275 (2000).